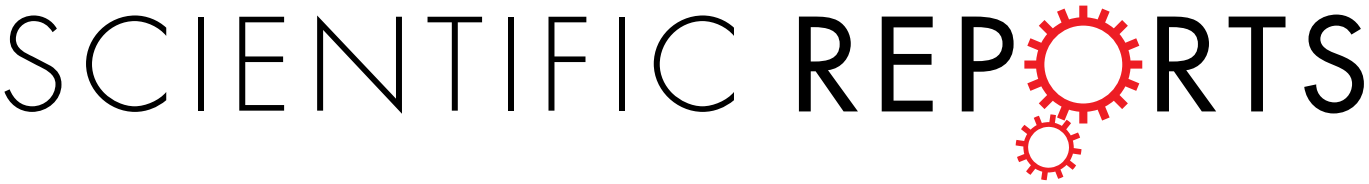

OPEN

Zircon U-Pb geochronology of crystal tuff on Lingshan Island and its geological implications for magmatism, stratigraphic age and geological events

Received: 9 November 2017
Accepted: 23 July 2018
Published online: 24 August 2018

Jindong Gao[1,3], Qiao Feng[2], Xiaoli Zhang[1], Lifa Zhou[1,3], Zunsheng Jiao[3,4] & Yu Qin[1]

Due to the unique location in the Ludong region, geochronological study of this area is essential for the understanding of the Cretaceous tectonic evolution of Eastern China. Sedimentary sequences interbedded with tuff layers unconformably overlay metamorphic rocks in the Sulu Orogen. This research presents a more reliable geochronological dataset of a tuff layer on Lingshan Island in Qingdao. A total of 103 valid age values from 216 zircon grains were obtained in three fresh tuff samples. Approximately 87% of these zircon ages are dated as the Early Cretaceous, and their peak ages shift from the Aptian stage to the Albian stage. The spatial-temporal relationship between the tuff and the Mesozoic igneous rocks of Eastern China indicate the impact of the Pacific Plate subduction beneath the Asian continent. Six Albian single detrital zircons have a weighted average age of 103.8 ± 1.4 Ma, with the youngest age (103.4 ± 1.4 Ma) constraining the maximum depositional age of the tuff layer. The age sequence of four sections on Lingshan Island is defined in this study: sections A and B belong to the Laiyang Group, and sections C and D are considered the Qingshan Group and were deposited in the Late Cretaceous. Two pre-Cretaceous zircon age peaks were also observed. These age peaks coincide with the magmatic and metamorphic ages preserved in the Sulu Orogen; thus, the Sulu Orogen is the provenance of the sedimentary rocks on Lingshan Island.

Convergent plate margins are the sites of most intense geological processes, such as magmatism, metamorphism, crust-mantle interactions, and related tectonic activity. Systematic geological, geochemical, and chronological analyses of the igneous rock groups exposed on the margins have provided important clues about the conditions required for the generation of magmas and the geodynamic evolution of an area[1–3]. Terrigenous clastic rocks, pyroclastic rocks, and volcanic lava overlay the ultrahigh-pressure (UHP) and high-pressure metamorphic rock and Yanshan granite in the Sulu Orogen[4,5]. Zhang *et al.* (2013) suggested that the lower strata on Lingshan Island should be the Lingshandao Formation (Fm.) because of the difference in lithology from the Laiyang Group[6]. Lu *et al.* (2011) and Feng *et al.* (2018) proposed that the lower part of the Lingshandao Fm. is a marine lithostratigraphic unit of the Jurassic to Cretaceous, rather than a part of the lacustrine Laiyang Group[7,8]. Li *et al.* (2017) confirmed the sedimentary strata lacustrine facies with the discovery of fish and conchostracan fossils and suggested that it should be the Fajiaying Formation of the Laiyang Group in the Jiaolai Basin[9]. Because the affiliation of the strata is controversial, further geochronology research is needed.

Surprisingly, a tuff layer almost 20.5 metres thick is interbedded in the Mesozoic strata on the Island and is referred to as rhyolite[7]. Based on the weighted mean of eleven concordant ages of 123.9 ± 1.6 Ma, Wang *et al.* (2014) suggested that this tuff was deposited in the Late Aptian[10]. This research presents new and more accurate

[1]State Key Laboratory of Continental Dynamics, Department of Geology, Northwest University, Xi'an, Shaanxi, 710069, China. [2]Qingdao National Laboratory for Marine Science and Technology, College of Earth Science and Engineering, Shandong University of Science and Technology, Qingdao, 266590, China. [3]Shaanxi Provincial Institute of Energy Resources & Chemical Engineering, Xi'an, Shaanxi, 710069, China. [4]School of Energy Resources, University of Wyoming, Laramie, Wyoming, 82017, USA. Jindong Gao and Qiao Feng contributed equally. Correspondence and requests for materials should be addressed to Q.F. (email: 13396251993@163.com)

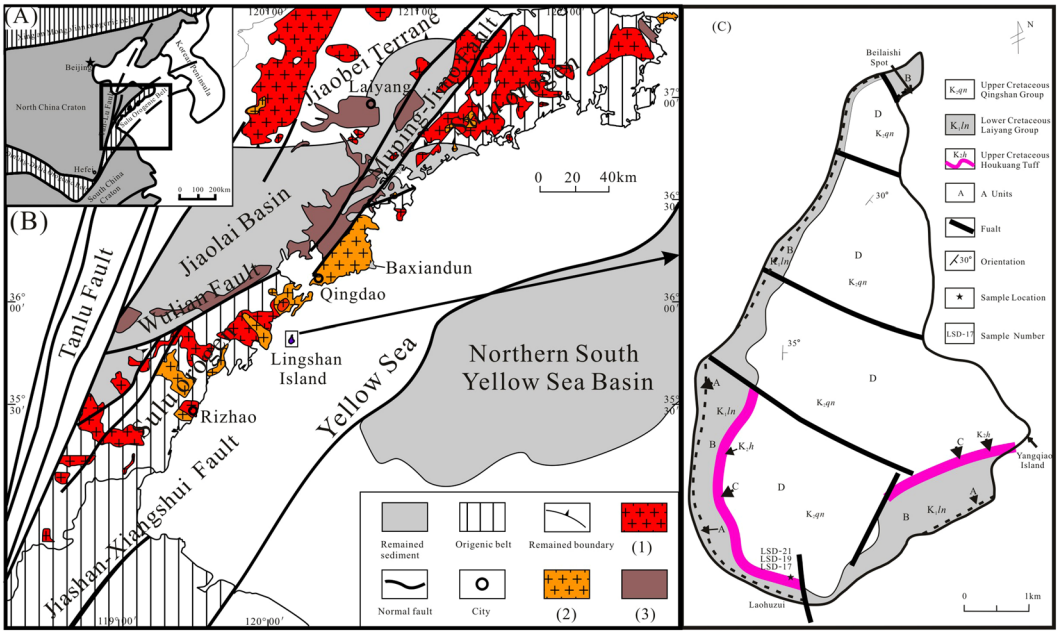

Figure 1. Simplified maps showing. (**A**) The location and tectonic setting of the Ludong area, China (modified after Suo *et al*. and Li *et al*.[87,88]). (**B**) The position of Lingshan Island and geological setting (modified after Suo *et al*. and Li *et al*.[87,88]). (**C**) The geological map of Lingshan Island showing sample locations (modified after Wang *et al*.[10]). And the legends in (**B**) are (1) Linglong granite; (2) Laoshan granite; (3) volcanic rocks.

tuff zircon geochronological data to further constrain the depositional age, and the spatial-temporal correlation between the strata exposed on Lingshan Island and the Mesozoic strata in the Jiaolai Basin. The new tuff zircon geochronological data also allow for mining the records of the pre and syn-collision evolution.

Geological Setting

The Sulu Orogen. The Sulu Orogen is the eastern extension of the Qinling–Dabie Orogen (truncated by the Tancheng-Lujiang Fault (TLF)) and developed as the result of the continental collision between the North China Craton (NCC) and the Yangtze Craton (YC) in the Early Triassic[11–13] (Fig. 1A). The UHP metamorphic rocks are predominantly granitic orthogneiss and enclosed eclogite and record the Neoproterozoic protolith ages and the metamorphism of Early Triassic[14,15]. The Sulu Orogen is not only one of the best-preserved and largest exposed ultrahigh-pressure metamorphic units in the world but also one of the areas that has suffered the most intense degree of magmatic activity during post-collisional exhumation[16,17]. In addition, the prevalent Mesozoic igneous rocks can be divided into 160 to 140 Ma granites represented by Linglong granite and 130–110 Ma granites represented by Laoshan granite (Fig. 1B). Moreover, terrestrial sedimentary rocks are comprised of clastic rocks, pyroclastic rocks, and volcanic lava, which unconformably overlay the UHP to high-pressure metamorphic rocks and Yanshan granite[5] (Fig. 1B). These strata are truncated by the Wulian-Muping-Jimo Fault and hence have been considered to be outcrops on the edge of the Jiaolai Basin[5] (Fig. 1B), whereas the lacustrine sedimentary rocks belong to the Laiyang Group, and the pyroclastic rocks in this area belong to the Qingshan Group.

Geological characteristics of the Jiaolai Basin and Lingshan Island. The Jiaolai Basin is a Mesozoic rift basin in which Early Cretaceous rocks unconformably overlay a Precambrian basement[18]. The stratigraphic sequences comprise the Early Cretaceous Laiyang Group, the Qingshan Group and the Late Cretaceous Wangshi Group, which represents a sequence of lacustrine clastic rock and volcanic rock assemblies[18–20]. Xie *et al*. (2012) and Zhang *et al*. (2004) obtained a maximum sedimentary age of 130 ± 2 Ma for the Laiyang Formation[18,21]. Zhang *et al*. (1996) provided a systematic chronologic analysis of 16 volcanic rocks from each interval of the Qingshan Group and concluded that the age of the Qingshan Group ranges from 125 to 98 Ma[22]. Ling *et al*. (2006) suggested that the age of the Qingshan Group ranges from 106 ± 2 to 98 ± 1 Ma based on a geochronologic study[23]. Qiu *et al*. (2001) concluded that the volcanic eruption age of the Qingshan Group ranges from 103.7 ± 2.8 to 94.0 ± 2.6 Ma[24]. Tang *et al*. (2008) concluded that the age of the Qingshan Group ranges from 118 to 93 Ma[25]. Kuang *et al*. (2012a,b) analysed the volcanic rocks of the Qingshan Group collected from the Qingdao, Jimo, Haiyang, Jiaozhou, Tancheng, Xiguanzhuang regions and concluded that the Qingshan Group ranges from 122 to 99 Ma, according to $^{40}Ar/^{39}Ar$ isotopic dating of whole rock[26,27].

Due to the similarly of the strata on Lingshan Island and in the Jiaolai Basin, the strata sequence of Lingshan Island can be divided into four sections (A to D) from bottom to top based on the characteristics of the rock assemblages (Supplementary Fig. 1). The features of these formations are described as follows.

Section A is mainly of dark grey sandstones interbedded with siltstones and mudstones. Graded-bedding, horizontal bedding (Supplementary Fig. 1a), Bouma sequences and small grooved cross-bedding are exhibited

and some structures, such as soft-sediment deformation and convolute bedding, occurr in this area[26]. The top strata overlay the section in a parallel unconformity (Supplementary Fig. 1b).

Yellow, thick-bedded, coarse-grained sandstone (Supplementary Fig. 1c) interbedded with fine sandstone, siltstone and dark mudstones are present in section B. Graded bedding and several convolute beds are exhibited. A Bouma sequence occurs at the top of this section (Supplementary Fig. 1d).

Section C is a thick, grey-white bedded felsic tuff with a maximum thickness of 20.5 m (Supplementary Fig. 1h). The tuff layer has horizontal bedding (Supplementary Fig. 1g) and large horizontal extension characters and conformably overlays Section B (Supplementary Fig. 1e), indicating the continuation of the lacustrine facies of section B[27,28].

Section D includes conglomerate, pebbly sandstones, sandstones (Supplementary Fig. 1l), grey mudstones, and volcanic rock (Supplementary Fig. 1m), and the upper part of this section mainly comprises volcanic rocks and volcaniclastic rocks (Supplementary Fig. 1o), and multiple mafic dikes. In addition, the uppermost layers incorporate conglomerate and pebbly sandstones (Supplementary Fig. 1n).

Sample Processing and Analysis

Petrography of samples. Samples LSD-17, LSD -19 and LSD-21 were collected in the tuff layer at the location of Laohuzui, which is located at the southernmost region of Lingshan Island (Fig. 1C and Supplementary Fig. 1).

Petrographic data indicates that the felsic tuff is mainly volcanic debris, with a small amount of terrestrial debris (Supplementary Fig. 1f,i,j,k). The tuff mainly comprises tephra (>80%) with a minor amount of volcanic breccia (<3%). The tephra is characteristically cuspate-shaped, sinuous and angular. Devitrified debris (<1 mm in diameter) represents a significant part of the rock (40~55%). Small broken quartz and feldspar clasts are interstitial to the matrix and volcanic breccia, and there are small amounts of plagioclase phenocrysts and anhedral grains of haematite in the matrix. Coarse-grained plagioclase phenocrysts are occasionally present and usually exhibit single twinning. Zircon, rutile, and haematite occur as accessory phases in the tuff.

Analytical methods. Zircons were selected in the Laboratory of the Mineral Geology Research Institute of the Langfang, Hebei Province. The zircon selection, reflected light and cathodoluminescence (CL) imaging, and zircon U-Pb isotope analyses were completed at the State Key Laboratory of Continental Dynamics at Northwest University in Xi'an, China. More detailed experimental procedures and methods can be found in Yuan *et al.*[29]. The obtained isotope ratio data was calculated using GLITTER 4.0 (Macquarie University), and the data was corrected using the external standard of the Harvard zircon 91500. Common Pb corrections were made using the 3D coordinate method following the method of Andersen[30]. Harmonic curve regression analysis was performed using ISOPLOT 3.0[31]. The age data of the zircon was rationally selected. Because zircon contains a large amount of radioactive Pb, $^{207}Pb/^{206}Pb$ age data was adopted for ancient zircons with ages of >1000 Ma, and $^{206}Pb/^{238}Pb$ age data was adopted for zircons with ages of <1000 Ma[29,32].

Analytical results. A total of 103 valid age values out of 216 zircon grains were obtained based on whether their U-Pb analyses were concordant or not. The geochronological data and their Th/U values are listed in Supplementary Tables 1, 2 and 3, and single zircon grain CL images are shown in Supplementary Fig. 2. U-Pb concordia diagrams and their corresponding relative probability plots of U-Pb ages are shown in Supplementary Fig. 3.

The zircons are euhedral and have length/width ratios ranging from one to three. Most zircons are brightly luminescent, with diameters less than 100 μm. Many zircons have retained their original crystal forms, strong oscillatory zoning and Th/U ratios ranging from 0.41 to 6.84, suggesting that they have a magmatic origin[33]. However, zircons 17–57, 21–17 and 21–71 appear homogeneous in CL images and were recorded to possess low Th/U ratios of 0.03, 0.08, and 0.08; these characteristics typically imply a metamorphic origin[34]. Several zircon grains exhibit anhedral dark cores and strong zoning. Supplementary Fig. 3 shows that the test data is concordant or nearly concordant, which suggests a minimal loss of Pb.

The Th/U ratios of the zircons from sample LSD-17 range from 0.48 to 5.22. The U and Th concentrations range from 36.67×10^{-6} to 3586.61×10^{-6} and from 56.44×10^{-6} to 9187.01×10^{-6}. The $^{206}Pb/^{238}Pb$ ages of the samples range from 104.6 ± 2.03 to 758.6 ± 6.79 Ma (Supplementary Fig. 3), and approximately 93.55% of these ages are concentrated between 139.3 and 104.6 Ma, with a peak age of 118.4 Ma.

As for sample LSD-19, more than 98% of the Th/U ratios are greater than 0.4, and the U and Th concentrations range from 41.85×10^{-6} to 1960.12×10^{-6} and 68.29×10^{-6} to 7323.1×10^{-6}, respectively. Their $^{206}Pb/^{238}Pb$ ages range from 103.6 ± 1.39 to 772 ± 9.05 Ma (Supplementary Fig. 3). Approximately 82.1% of these ages are concentrated between 134.6 and 103.6 Ma, with a peak age of 118.2 Ma.

More than 96% of the Th/U ratios are greater than 0.4 for sample LSD-21. In addition, the U and Th concentrations range from 97.09×10^{-6} to 1938.96×10^{-6} and from 31.47×10^{-6} to 5694.25×10^{-6}, respectively. Their $^{206}Pb/^{238}Pb$ ages range from 103.4 ± 1.4 to 769.7 ± 7.44 Ma (Supplementary Fig. 3). Approximately 87.27% of these ages are concentrated between 131.6 to 103.4 Ma, with a peak age of 110.4 Ma.

Overall, more than 80% of the zircon ages are within the Early Cretaceous, with the other recorded ages are older than the Early Cretaceous.

Discussion

Detrital zircon geochronological research has become a hot topic of global research, as it has been widely used to constrain stratigraphic ages, perform provenance analysis, and provide the inverse analysis of tectonic thermal evolution[35–40]. As products of volcanic activity, tuff layers often exhibit stable distribution and instantaneous deposition. As a result, they are usually regarded as key beds for stratigraphic correlation[41,42]. Moreover, tuff zircon

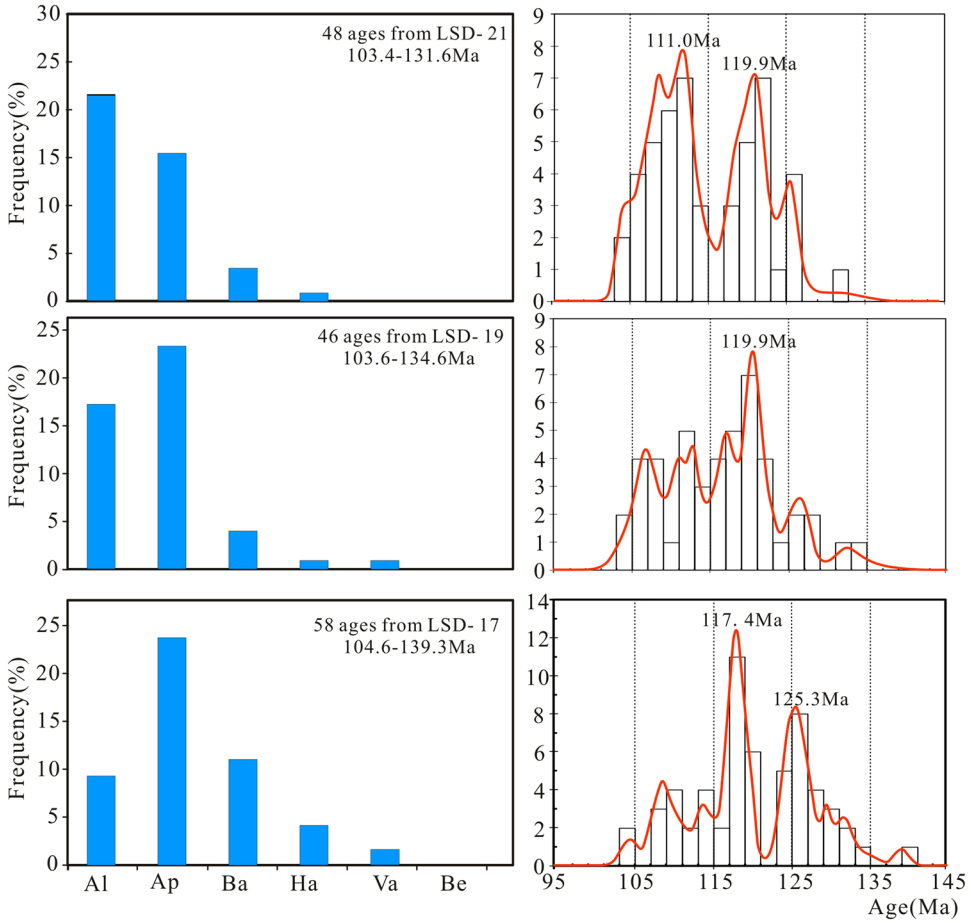

Figure 2. Age-probability plot of the early Cretaceous zircon grains. Notes: Al: Albain; Ap: Aptain; Ba: Barremian; Ha: Hauterivian; Va: Valanginian; Be: Berriasian.

chronology is most useful when obtaining the numerical ages for tephra or transported cryptotephra, although dating the cryptotephra with a high degree of likelihood using stratigraphy and comparisons by matching the inherent compositional features of deposits is common. Hence, this approach is an age equivalent dating method that provides an exceptionally precise volcanic event stratigraphy. Such age transfers are valid because the primary tephra deposits from an eruption essentially have the same short-lived age everywhere they occur and form isochrons quickly after an eruption (normally within one year)[43–47].

Interpretation of age data. As shown in Fig. 2, the Early Cretaceous zircon age displays the following characteristics: (1) The main peak age shifts from the Aptian stage to the Albian stage; (2) the amount of zircon increases from the Berriasian stage to the Albain stage. The age ranges of the three samples are 104.6 Ma to 139.3 Ma, 103.6 Ma to 134.6 Ma, and 103.4 Ma to 131.6 Ma, respectively, showing that both the maximum and minimum age values decrease as the sample location transitions from the bottom to the top (Fig. 2). These characteristics suggest that these ages are consistent with Smith's law of stratigraphic superposition[48], which further supports the accuracy of the obtained age data.

Three peak ages were recorded for the early Cretaceous zircons: ~125.3 Ma, ~119.9 Ma, and ~111.0 Ma (Fig. 2). These age peaks indicate three states of magma condensation and zircon crystallization. Goss *et al*. (2010) obtained a SHRIMP U-Pb age of 115 ± 2 Ma for the Laoshan granite in the Sulu Orogen[49]. That age is the same as the peak age of the Early Cretaceous zircons in our study. Moreover, Early Cretaceous magmatism was widespread throughout Eastern China (Supplementary Table 4) and possesses a NEE directional distribution that diminishes to the west[50–52]. Almost at the same time, the rift basins of China became widely developed[18,53]. All of these facts indicate that the Early Cretaceous magmatism was most likely related to the subduction of the Pacific Plate beneath the Asian continent[18,54]. Therefore, the obtained main age peaks of 125.3 to 111.0 Ma may reflect the background of large scale magmatic activity in Eastern China.

Age determination of tuff strata. Four methods using detrital zircon to constrain the maximum depositional age were employed in previous studies: (1) the weighted average age of the zircons[1,55–57]; (2) the youngest graphical detrital zircon age[32,58–60]; (3) the youngest detrital zircon age, which is calculated using Isoplot[31,60]; and (4) the youngest single detrital zircon age[61–66]. Because the crystallization of the tuff zircon should be earlier than

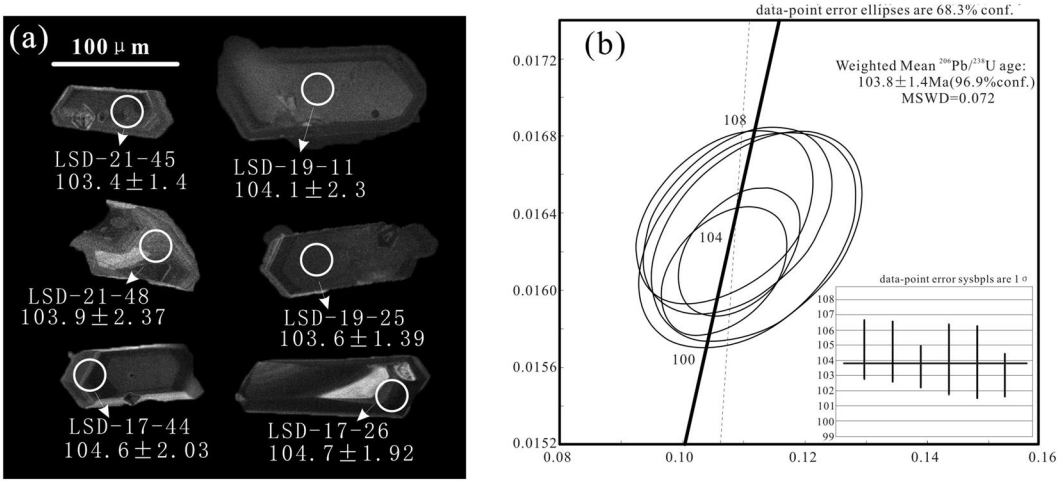

Figure 3. Cathodoluminescence (CL) images of Zircon grains (**a**) and U–Pb concordia diagrams and weighted mean ages in Albian stage (**b**).

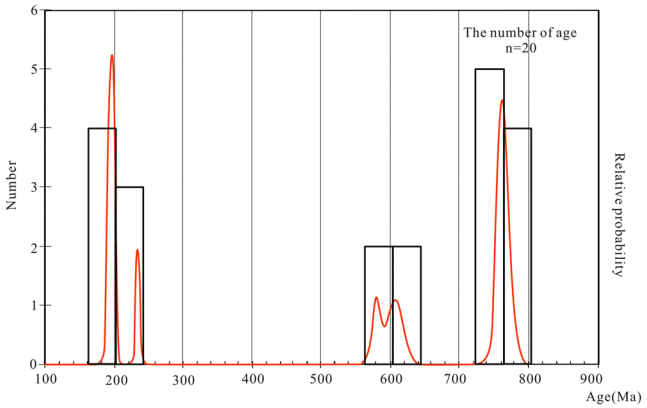

Figure 4. Age-probability plot and age-distribution curve of the pre-Cretaceous zircon grain.

or contemporaneous with the volcanic eruption and the deposition should be later than the volcanic eruption, the youngest single detrital zircon age is the most reasonable for constraining the maximum depositional age[62,67].

Six single detrital zircons were observed with clear oscillatory zoning within the Albian stage. These ages were 103.4 ± 1.4 Ma, 104.1 ± 2.3 Ma, 103.9 ± 2.37 Ma, 103.6 ± 1.39 Ma, 104.6 ± 2.03 Ma, and 104.7 ± 1.92 Ma (Fig. 3a) with a weighted average age of 103.8 ± 1.4 Ma (Fig. 3b). The Th/U ratios were 1.66, 1.05, 1.76, 2.03, 1.96, and 4.17. Ling *et al.* (2006) acquired a weighted average age of the Houkuang Formation of the Qingshan Group in the Jiaolai Basin of 106 Ma[23]. This age is consistent with the obtained age in this research. The youngest single detrital zircon age (103.4 ± 1.4 Ma) constrains the maximum depositional age of the tuff layer, which means that the depositional age of this formation should not be earlier than the Albian period. The age 103.4 ± 1.4 Ma is very close to the boundary age (100.5 Ma) between the Early and Late Cretaceous (ICC, 2015). Moreover, the minimum age of the Qingshan Group is approximately 98 ± 1 Ma[23]. Thus, sections A and B and the Laiyang Group in the Jiaolai Basin were likely deposited in the Early Cretaceous, and sections C and D belong to the Qingshan Group, which was deposited in the Late Cretaceous. This conclusion is different from the hypothesis that the Qingshan Group in the Jiaolai Basin was deposited in the Early Cretaceous and is also different from the conclusion of Wang *et al.* (2014).

Regional geological events and sediment provenance. Magmatic activity and metamorphism represent two important records that can be used to determine regional geological events. The geochemical analysis of zircon allows insight into regional volcanic and magmatic processe and also provides an inverse analysis of the tectonic thermal evolution and a sedimentary provenance analysis[68,69]. In this study, we observed two pre-Cretaceous zircon age peaks (Fig. 4), which indicate the prior occurrence of magmatic activity and metamorphism. The ages of the pre-Cretaceous zircons on Lingshan Island coincide with the ages of the pre- and syn-collisional magmatic and metamorphic events[12,70–76].

Precambrian tectonic thermal event (845–582 Ma). The Precambrian zircons have two secondary peak ages, Early Sinian (772 to 742 Ma) and Late Sinian (609 to 578 Ma) (Fig. 4). An obvious core-rim structure and strong

oscillatory zoning indicates that these zircons are of magmatic origin. Granitic orthogneiss with the protolith age of 780 to 570 Ma is widely distributed in the South Sulu Orogen, which indicates that Neoproterozoic magmatic activity was prevalent in the South China Plate[11,12,14,77–79]. The obtained ages are consistent with the age record in the Sulu Orogen. Zheng *et al.* (2013) suggested that Neoproterozoic granitic magma has a characteristic double peak[15]. Geochemical analysis indicated that the magmatic activity was likely related to the breakup of the supercontinent Rodinia[14,80,81].

Triassic-Jurassic tectonic events. There are two secondary peak ages, Triassic and Jurassic. The three individual zircons of Triassic age in this study are 234 ± 2.4 Ma, 206.7 ± 5.1 Ma, and 201.4 ± 1.32 Ma. These zircons are considered to have a metamorphic origin based on their unclear zoning, high degrees of roundness, and low Th/U ratios. Geochronologic values in the Sulu Orogen indicate that the age peak of the high-pressure rocks is 260 to 245 Ma and that their degenerative age is 253 to 210 Ma; the metamorphism peak age of the UHP rocks is 240 to 225 Ma, and their degenerative age is 220 to 200 Ma[76,77,82]. The Triassic detrital zircon obtained in this research is consistent with the metamorphic age, which further supports the age of the continental collision between the North China Plate and South China Plate.

There are five Jurassic zircons with a peak age of 192.1 Ma. These zircons exhibit clear zoning, which reflects their magmatic origin. Lin *et al.* (2000) and Xu *et al.* (2002) reported an Early Jurassic intrusive complex with an age of 191 Ma[83,84]. Zhai *et al.* (2005) suggested that the granite and neutral intrusive rocks formed in the North China Craton at 210 to 180 Ma[85]. These rocks may record the earliest evidence of lithospheric thinning and mantle hydrothermal activity that occurred after the collision of the Sulu Orogen[86].

Conclusion

(1) The Cretaceous sequence on Lingshan Island is similar to the sedimentary strata assembly in the Jiaolai Basin and is divided into four sections: A, B, C, and D. Section C is a grey tuff layer with a maximum thickness of 20.5 m; the tuff layer possesses lacustrine horizontal facies bedding mainly composed of tephra (>80%) and a minor amount of volcanic breccia (<3%).

(2) A total of 103 valid age values out of 216 zircon grains were obtained from three fresh tuff samples. More than 87% of these zircons were dated to the Early Cretaceous. The spatial-temporal relationship between the tuff and Early Cretaceous magmatism of the Ludong area indicate the likelihood of the subduction of the Pacific Plate beneath the Asian continent.

(3) Six single detrital zircons within the Albian stage yielded a weighted average age of 103.8 ± 1.4 Ma, with the youngest single detrital zircon age recorded at 103.4 ± 1.4 Ma. The youngest single detrital zircon age is very close to the boundary age (100.5 Ma) between the Early and Late Cretaceous. Thus, sections A and B and the Laiyang Group in the Jiaolai Basin were deposited in the Early Cretaceous, whereas sections C and D belong to the Qingshan Group and were deposited in the Late Cretaceous.

(4) Pre-Cretaceous single zircon ages are mainly distributed throughout the Neoproterozoic and Triassic-Jurassic. The Precambrian zircons are likely related to the breakup of the supercontinent Rodinia; the Triassic metamorphic zircons support the geological age of the collision between the North China Plate and the South China Plate, and the Jurassic zircons record the earliest evidence of lithospheric thinning and mantle hydrothermal activity that occurred after the collision of the Sulu orogeny. These facts indicate that the Sulu Orogen is a coeval source provenance of the sedimentary rocks on Lingshan Island.

References

1. Eyuboglu, Y. Petrogenesis and U-Pb zircon chronology of felsic tuffs interbedded with turbidites (Eastern Pontides Orogenic Belt, NE Turkey): Implications for Mesozoic geodynamic evolution of the eastern Mediterranean region and accumulation rates of turbidite sequen. *J. Lithos.* **212–215**, 74–92 (2015).
2. Feng, Q., Qin, Y., Fu, S. T., Liu, Y. Q. & Zhou, D. W. The Enrichment of Calcite and the Genesis of Uranium Deposits in Dongsheng Uranium Sandstone. *J. Geological Journal of China Universities.* **22**(1), 053–059 (2016).
3. Zhou, S. C. *et al.* Sedimentary environments of the Middle Ordovician Pingliang Formation in the Qishan section, southern Ordos Basin. *J. Sedimentary Geology and Tethyan Geology.* **31**(4), 28–33 (2011).
4. Sun, D., Feng, Q., Liu, Z., Lu, C. J. & Lu, X. Detrital Zircon U-Pb Dating of the Upper Triassic Yanchang Formation in Southwestern Ordos Basin and Its Provenance Significance. *J. Acta Geologica Sinica.* **91**(11), 2521–2544 (2017).
5. Zhou, Y. Q., Zhang, Z. K., Liang, W. D., Li, S. & Yue, H. W. Late Mesozoic tectono-magmatic activities and prototype basin recovery in eastern shandong province. *J. Earth Science Frontiers.* **22**(1), 137–156 (2015).
6. Zhang, H. C. *et al.* The Lingshandao Formation: a new lithostratigraphic unit of the Lower Cretaceous in Qingdao, Shandong, China. *J. Stratigr.* **37**, 196–202 (2013).
7. Lu, H. B., Wang, J. & Zhang, H. C. Discovery of the Late Mesozoic Slump Beds in Lingshan Island, Shandong, and a Pilot Research on the Regional Tectonics. *J. Acta Geol Sinica.* **85**, 938–946 (2011).
8. Feng, Q. *et al.* Geochemical characteristics and paleoevironmental analysis of dark finegrained rocks of Wawukuang and Shuinan formations in Jiaolai basin. *J. Journal of Shandong University of Science and technology (Natural Science).* **37**(1), 20–34 (2018).
9. Li, S. J. *et al.* Discovery of fish and conchostracan fossils in Lower cretaceous in Lingshan Island, Qingdao, Shandong. *J. Geological review.* **63**(1), 1–6 (2017).
10. Wang, J., Chang, S. C., Lu, H. B. & Zhang, H. C. Detrital zircon U-Pb age constraints on Cretaceous sedimentary rocks of Lingshan Island and implications for tectonic evolution of Eastern Shandong, North China. *J. Journal of Asian Earth Sciences.* **96**, 27–45 (2014).
11. Ames, L., Tilton, G. R. & Zhou, G. Timing of collision of the Sino-Korean and Yangtze cratons: U-Pb zircon dating of coesite-bearing eclogites. *J. Geology.* **21**, 339–342 (1993).
12. Hacker, B. R., Wallis, S. R., Ratschbacher, L., Grove, M. & Gehrels, G. High-temperature geochronology constraints on the tectonic history and architecture of the ultra-highpressure Dabie–Sulu orogen. *J. Tectonics.* **25**, TC5006 (2006).
13. Zheng, Y. F. Metamorphic chemical geodynamics in continental subduction zones. *J. Chemical Geology.* **328**, 5–48 (2012).

14. Xu, Z. Q. *et al*. Deep Subduction Erosion Model for Continent-Continent Collision of the Sulu HP-UHP Metamorphic Terrain. *J. Earth Science*. **31**(4), 427–435 (2006).
15. Zheng, Y. F., Xiao, W. J. & Zhao, G. C. Introduction to tectonics of China. *J. Gondwana Res*. **23**, 1189–1206 (2013).
16. Zhao, Z. F., Zheng, Y. F., Wei, C. S. & Wu, Y. B. Post-collisional granitoids from the Dabie orogen in China: Zircon U-Pb age, element and O isotope evidence for recycling of subducted continental crust. *J. Lithos*. **93**, 248–272 (2007).
17. Zhang, J., Zhao, Z. F., Zheng, Y. F. & Dai, M. Postcollisional magmatism: Geochemical constraints on the petrogenesis of Mesozoic granitoids in the Sulu orogen, China. *J. Lithos*. **119**, 512–536 (2010).
18. Zhang, Y. Q., Zhao, Y., Dong, S. W. & Yang, N. Tectonic evolution stages of the Early Cretaceous rift basin s in Eastern China and adjacent areas and their geodynamic background. *J. Earth Science Frontier* **11**(3), 123–132 (2004).
19. Wang, Q. Y. *et al*. Parasequence analysis of the field outcrop sections based on the sedimentary microfacies analysis: An example from the Ordovician Majiagou Formation in Linfen, eastern Ordos Basin. *J. Sedimentary Geology and Tethyan Geology* **34**(02), 18–28 (2014).
20. Cao., J. Z. *et al*. Sequence Stratigraphy of Ordovician Strata in the South Part of Ordos Area. *J. Acta Sedimentologica Sinica* **29**(02), 286–292 (2011).
21. Xie, S. *et al*. U-Pb ages and trace elements of detrital zircons from Early Cretaceous sedimentary rocks in the Jiaolai Basin, north margin of the Sulu UHP terrane: Provenances and tectonic implications. *J. Lithos*. **154**(1), 346–360 (2012).
22. Zhang, Z. Q. & Liu, M. W. Rock formation of Shandong Provence. 200–251 (China University of geosciences press, 1996).
23. Ling, W. L., Xie, X. J., Liu, X. M. & Cheng, J. P. Zircon U-Pb dating on the Mesozoic volcanic suite from the Qingshan Group stratotype section in eastern Shandong Province and its tectonic significance. *J. Science in China (Series D)*. **36**(5), 401–411 (2006).
24. Qiu, J. S., Wang, D. Z. & Luo, Q. H. ^{40}Ar-^{39}Ar dating for volcanic rocks of Qingshan formation in Jiaolai basin, eastern Shandong Province: A case study of the Fenlingshan volcanic apparatus in Wulian county. *J. Geological Journal of China Universities*. **7**(3), 351–355 (2001).
25. Tang, J. F., Liu, Y. L. & Wang, Q. F. Geochronology of Mesozoic vocanic rocks in Shandong Provence. *J. Acta Petrologica Sinica*. **24**(6), 1333–1338 (2008).
26. Kuang, Y. S., Pang, C. J., Hong, L. B., Zhong, Y. T. & Xu, Y. G. Geochronology and Geochemistry of the Late Cretaceous Basalts in the Jiaolai Basin: Constraints on lithospheric thinning and accretion beneath North China Craton. *J. Journal of geotectonics and metallogeny*. **36**(4), 559–571 (2012a).
27. Kuang, Y. S. *et al*. ^{40}Ar-^{39}Ar geochronology and geochemistry of mafic rocks from Qingshan Group, Jiaodong area: Implications for the destruction of the North China Craton. *J. Acta Petrologica Sinica*. **28**(4), 1073–1091 (2012b).
28. Li, Y. L. *et al*. Neogene sedimentary facies and palaeogeography of western Qaidam Basin, Qinghai. *J. Sedimentary Geology and Tethyan Geology* **32**(02), 31–36 (2012).
29. Yuan, H. L. *et al*. Determination of U-Pb age and rare earth element concentrations of zircons from Cenozoic untrusions in northeastern China by laser ablation ICP-MS. Chin. *J. Sci. Bull*. **48**, 1511–1520 (2003).
30. Andersen, T. Correction of common lead in U-Pb analyses that do not report ^{204}Pb. *J. Chemical Geology*. **192**, 59–79 (2002).
31. Ludwig, K. R. User's manual for isoplot/ex version 3.00-a geochronology toolkit for Microsoft excel, No. 4. Z. Berkeley Geochronological Center, Special Publication, 1–70 (2003).
32. Gao, S. *et al*. Determination of Forty Two Major and Trace Elements in USGS and NIST SRM Glasses by Laser Ablation-Inductively Coupled Plasma-Mass Spectrometry. *J. Geostandards & Geoanalytical Research*. **26**(2), 181–196 (2002).
33. Rubatto, D. Zircon trace element geochemistry: partitioning with garnet and the link between U-Pb ages and metamorphism. *J. Chemical Geology*. **184**(1–2), 123–138 (2002).
34. Pidgeon, R. T. & Wilde, S. A. The interpretation of complex zircon U-Pb systems in Archaean granitoids and gneisses from the Jack Hills, Narryer Gneiss Terrane, Western Australia. *J. Precambrian Research*. **91**(91), 309–332 (1998).
35. Nelson, D. R. An assessment of the determination of depositional ages for Precambrian clastic sedimentary rocks by U-Pb dating of detrital zircons. *J. Sedimentary Geology*. **s141–142**, 37–60 (2001).
36. Tucker, R. T., Roberts, E. M., Hu, Y., Kemp, A. I. S. & Salisbury, S. W. Detrital zircon age constraints for the Winton Formation, Queensland: Contextualizing Australia's Late Cretaceous dinosaur faunas. *J. Gondwana Research*. **24**(2), 767–779 (2013).
37. Li, X. H., Li, Z. X. & Li, W. X. Detrital zircon U-Pb age and Hf isotope constrains on the generation and reworking of Precambrian continental crust in the Cathaysia Block, South China: A synthesis. *J. Gondwana Research*. **25**, 1202–1215 (2014).
38. Feng, Q. *et al*. U-Pb age of detrital zircons and its geological significance from Maoniushan Formation in the Wulan County, northern margin of Qaidam Basin. *J. Acta Sedimentologica Sinica*. **33**(3), 487–499 (2015).
39. Qin, Y. *et al*. Devonian post-orogenic extension-related volcano-sedimentary rocks in the northern margin of the Tibetan Plateau, NW China: Implications for the Paleozoic tectonic transition in the North Qaidam Orogen. *J. Journal of Asian Earth Sciences*. **156**, 145–166 (2018).
40. Bhattacharya, J. P., Copeland, P., Lawton, T. F. & Holbrook, J. Estimation of source area, river paleo-discharge, paleoslope, and sediment budgets of linked deep-time depositional systems and implications for hydrocarbons potential. *J. Earth-Science Reviews*. **153**, 77–110 (2016).
41. Takeshita, Y., Matsushima, N., Teradaira, H., Uchiyama, T. & Kumai, H. A marker tephra bed close to the Lower-Middle Pleistocene boundary: Distribution of the Ontake-Byakubi Tephra Bed in central Japan. *J. Quaternary International*. **397**, 27–38 (2015).
42. Albert, P. G. *et al*. Glass geochemistry of pyroclastic deposits from the Aeolian Islands in the last 50 ka: A proximal database for tephrochronology. *J. Journal of Volcanology and Geothermal Research*. **397**, 1–27 (2017).
43. Mills, M. J. Volcanic aerosol and global atmospheric effects (Ed. Sigurdsson, H.) 931–943 (Encyclopaedia of Volcanoes. Academic Press, San Diego, CA, 2000).
44. Rose, W. I. & Durant, A. J. Fine ash content of explosive eruptions. *J. Journal of Volcanology and Geothermal Research*. **186**, 32–39 (2009).
45. Bourne, A. *et al*. Distal tephra record for the last 105, 000 years from the core PRAD 1–2 in the Adriatic Sea: implications for marine tephrostratigraphy. *J. Quat. Sci. Rev*. **29**(23–24), 1–16 (2010).
46. Bourne, A. J. *et al*. Tephrochronology of core PRAD1-2 from the Adriatic Sea: insights into Italian explosive volcanism for the period 200–80. *J. Quat. Sci. Rev*. **116**, 28–43 (2015).
47. Matthews, I. P. *et al*. Developing a robust tephrochronological framework for Late Quaternary marine records in the Southern Adriatic Sea: new data from core station SA03-11. *J. Quat. Sci. Rev*. **118**, 84–104 (2015).
48. Du, Y. S. & Zhang, K. X. Discussions on non-Smith stratigraphy. *J. Journal of Stratigraphy*. **23**(1), 78–80 (1999).
49. Goss, S. C., Wilde, S. A., Wu, F. & Yang, J. The age, isotopic signature and significance of the youngest Mesozoic granitoids in the Jiaodong Terrane, Shandong Province, North China Craton. *J. Lithos*. **120**(3–4), 309–326 (2010).
50. Sato, K. *et al*. Mid-Cretaceous episodic magmatism and tin mineralization in Khingan-Okhotsk volcano- plutonic belt, fareast Russia. *J. Resour. Geol*. **52**, 1–14 (2002).
51. Wu, F. Y., Lin, J. Q., Wilde, S. A., Zhang, X. & Yang, J. H. Nature and significance of the Early Cretaceous giant igneous event in eastern China. *J. Earth & Planetary Science Letters*. **233**(1), 103–119 (2005).
52. Ratschbacher, L. *et al*. Tectonics of the Qinling (Central China): tectonostratigraphy, geochronology, and deformation history. *J. Tectonophysics*. **366**, 1–53 (2003).
53. Yang, Q., Santosh, M., Shen, J. & Li, S. Juvenile vs. recycled crust in NE China: Zircon U-Pb geochronology, Hf isotope and an integrated model for Mesozoic gold mineralization in the Jiaodong Peninsula. *J. Gondwana Research*. **25**(4), 1445–1468 (2014).

54. Fu, W. Z. *et al*. Geochemical Characteristics of Volcanic Rocks in Cretaceous Qingshan Group from Southern Margin of Jiaolai Basin, Shandong Province. *J. Acta Geologica Sinica.* **88**(6), 1106–1119 (2014).
55. Gao, L. Z. *et al*. Geochronographic dating of the Tieshajie Formation in the Jiang-Shao fault zone and its implications. *J. Geological Bulletin of China.* **32**(7), 996–1005 (2013).
56. Dai, J. *et al*. Multi-stage volcanic activities and geodynamic evolution of the Lhasa terrane during the Cretaceous: Insights from the Xigaze forearc basin. *J. Lithos.* **s218–219**, 127–140 (2015).
57. Zhao, L. L. *et al*. Geochemistry and zircon U-Pb geochronology of the rhyolitic tuff on Port Island, Hong Kong: implications for early Cretaceous tectonic setting. *J. Geoscience Frontiers.* **8**(3), 565–581 (2017).
58. Cho, M., Cheong, W., Ernst, W. G. & Kim, J. SHRIMP U-Pb ages of detrital zircons in metasedimentary rocks of the central Ogcheon fold-thrust belt, Korea: Evidence for tectonic assembly of Paleozoic sedimentary protoliths. *J. Journal of Asian Earth Sciences.* **63**, 234–249 (2013).
59. Ghiglione, M. C. *et al*. U-Pb zircon ages from the northern Austral basin and their correlation with the Early Cretaceous exhumation and volcanism of Patagonia. *J. Cretaceous Research.* **55**, 116–128 (2015).
60. Li, Z. H. *et al*. Chronology and its significance of the Lower Jurassic tuff in Ordos Basin and its periphery. *J. Oil & Gas Geology.* **35**(3), 729–741 (2014).
61. Surpless, K. D., Graham, S. A., Covault, J. A. & Wooden, J. L. Does the Great Valley Group contain Jurassic strata? Reevaluation of the age and early evolution of a classic foreland basin. *J. Geology.* **34**, 21–24 (2006).
62. Brown, E. R. & Gehrels, G. E. Detrital zircon constraints on terrane ages and affinities and timing of orogenic events in the San Juan Islands and North Cascades, Washington. Can. *J. Earth Sci.* **44**, 1375–1396 (2007).
63. Dickinson, W. R. & Gehrels, G. E. Sediment delivery to the Cordilleran foreland basin: Insights from U-Pb ages of detrital zircons in Upper Jurassic and Cretaceous strata of the Colorado Plateau. Am. *J. Sci.* **308**, 1041–1082 (2008a).
64. Dickinson, W. R. & Gehrels, G. E. U-Pb ages of detrital zircons in relation to paleogeography: Triassic paleodrainage networks and sediment dispersal across southwest Laurentia. *J. Sediment. Res.* **78**, 745–764 (2008b).
65. Dickinson, W. R. & Gehrels, G. E. U-Pb ages of detrital zircons in Jurassic eolian and associated sandstones of the Colorado Plateau: evidence for transcontinental dispersal and intraregional recycling of sediment. *J. Geol. Soc. Am. Bull.* **121**, 408–433 (2009a).
66. Dickinson, W. R. & George, E. Gehrels. Use of U-Pb ages of detrital zircons to infer maximum depositional ages of strata: A test against a Colorado Plateau Mesozoic database. *J. Earth and Planetary Science Letters.* **288**, 115–125 (2009b).
67. Andersen, T. Detrital zircons as tracers of sedimentary provenance: limiting conditions from statistics and numerical simulation. *J. Chemical Geology.* **216**, 249–270 (2005).
68. Lowe, D. J. Tephrochronology and its application: A review. *J. Quatemary Geochronology.* **6**(2), 107–153 (2011).
69. Zhao Z. F. & Zheng, Y. F. Granite inherited zircon causes and nature of the magma source area in continental collision orogenic belt. *C. The symposium of isotope chronology isotope geochemistry* 2285–2289 (2013).
70. Yang, J. S. *et al*. SHRIMP U-Pb dating of coesite-bearing zircon from the ultrahigh-pressure metamorphic rocks, Sulu terrane, east China. *J. Journal of Metamorphic Geology.* **21**(21), 551–560 (2010).
71. Yang, J. S. *et al*. Genesis of garnet peridotites in the Sulu UHP belt: examples from the Chinese continental scientific drilling project-main hole, PP1 and PP3 drillholes. *J. Tectonophysics.* **475**, 359–382 (2009).
72. Yang, J. S. *et al*. Two ultrahigh - pressure metamorphic events recognized in the Central Orogenic Belt of China: evidence from the U-Pb dating of coesite-bearing zircons. *J. International Geology Review.* **47**, 327–343 (2005).
73. Xu, Z. Q. Continental deep subduction and exhumation dynamics: Evidence from the main hole of the Chinese Continental Scientific Drilling and the Sulu HP-UHP metamorphic terrane. *J. Acta Petrologica Sinica.* **23**(12), 3041–3053 (2007).
74. Katsube, A., Hayasaka, Y., Santosh, M., Li, S. & Terada, K. SHRIMP zircon U-Pb ages of eclogite and orthogneiss from Sulu ultrahigh-pressure zone in Yangkou area, eastern China. *J. Gondwana Research.* **15**(2), 168–177 (2009).
75. Chen, Y. X., Zhou, K., Zheng, Y. F. & Hu, Z. Garnet geochemistry records the action of metamorphic fluids in ultrahigh-pressure dioritic gneiss from the Sulu orogen. *J. Chemical Geology.* **398**, 46–60 (2015).
76. He, Q., Zhang, S. B. & Zheng, Y. F. High temperature glacial meltwater-rock reaction in the Neoproterozoic: evidence from zircon *in-situ* oxygen isotopes in granitic gneiss from the Sulu orogen. *J. Precambrian Research.* **284**, 1–13 (2016).
77. Wu, Y. B., Zheng, Y. F. & Zhou, J. B. Neoproterozoic granitoid in northwest Sulu and its bearing on the North China-South China Block boundary in east China. *J. Geophys Res Lett.* **31**(7), 157–175 (2004).
78. Xu, Z. Q. *et al*. Record for Rodinia supercontinent breakup event in the south Sulu ultra-high pressure metamorphic terrane. *J. Acta Petrologica Sinica.* **22**(7), 1745–1760 (2006).
79. Wang, X. X., Wang, T. & Zhang, C. L. Neoproterozoic, Paleozoic, and Mesozoic granitoid magmatism in the Qinling Orogen, China: Constraints on orogenic process. *J. Asian Earth Sci.* **72**, 129–151 (2013).
80. Lu, S. N. *et al*. Meso-Neoproterozoic Geological Evolution in the Qinling Orogeny and its Response to the Supercontinental Events of Rodinia. 94–116 (Geological Publishing House, Beijing, 2003).
81. Zhou, J., Li, X. H., Ge, W. & Li, Z. X. Age and origin of middle Neoproterozoic mafic magmatism in southern Yangtze Block and relevance to the break-up of Rodinia. *J. Gondwana Research.* **12**, 184–197 (2007).
82. Eide, E. A., Mcwilliams, M. O. & Liou, J. G. $^{40}Ar/^{39}Ar$ geochronology and exhumation of high-pressure to ultrahigh -pressure metamorphic rocks in east-central China. *J. Geology.* **22**(7), 601–604 (1994).
83. Lin, J. Q., Tan, D. J., Li, J. H. & Liu, Z. S. Early Jurassic Banjing instrusive complex of southern marginal zone of North China block, Xuzhou. *J. Journal of Changchun University of Science and Technology.* **30**(3), 209–214 (2000).
84. Xu, W. L., Wang, D. Y., Liu, X. C., Wang, Q. H. & Lin, J. Q. Discovery of eclogite inclusion sand its geological significance in early Jurassic intrusive complex in Xuzhou, northern Anhui, eastern China. *J. Chinese Sci. Bull.* **47**(14), 1212–1217 (2002).
85. Zhai, M. G., Fan, Q. C., Zhang, H. F. & Sui, J. L. Lower crustal processes in the lithospheric thinning: magma underplating, replacement and delamination. *J. Acta Petrol Sin.* **21**, 1509–1526 (2005).
86. Zhang, Q., Jin, W. J., Li, C. D. & Wang, Y. L. Yanshanian large-scale magmatism and lithosphere thinning in Eastern China: Relation to large igneous province. *J. Earth Sci Front.* **16**, 21–51 (2009).
87. Suo, Y. H., Li, S. Z., Dai, L. M., Liu, X. & Zhou, L. H. Cenozoic tectonic migration and basin evolution in East Asia and its continental margins. *J. Acta Petrologica Sinica.* **28**(8), 2602–2618 (2012).
88. Li, S. *et al*. Triassic southeastward subduction of North China Block to South China Block: Insights from new geological, geophysical and geochemical data. *J. Earth-Science Reviews.* **166**, 270–285 (2017).

Acknowledgements

This work was co-supported by the National Natural Science Foundation of China (41428201) and National Science, Technology Major Project (2016ZX05003006) and National key R&D program of China (2016YFE0102500).

Author Contributions

Qiao Feng and Jindong Gao designed the study with great help and comments from Xiaoli Zhang, Lifa Zhou, Zunsheng Jiao and Yu Qin. Qiao Feng and Jindong Gao took the field samples, performed the experiments and carried out data analysis. Jindong Gao wrote the manuscipt.

Additional Information

Supplementary information accompanies this paper at https://doi.org/10.1038/s41598-018-30060-1.

Competing Interests: The authors declare no competing interests.

Publisher's note: Springer Nature remains neutral with regard to jurisdictional claims in published maps and institutional affiliations.